Detection and Localization of Edges in Textured Images Modeled by Gaussian Markov Random Fields†

Fernand Cohen*, Yunhe Liu*, and Zhigang Fan**

* Department of Electrical and Computer Engineering, Drexel University, Philadelphia, PA 19104
** Xerox Corporation, Webster Research Center, 128-29E, Webster, NY 14580, USA

RÉSUMÉ

A new edge-based algorithm is presented for segmenting textured images modeled by Gaussian Markov Random Fields (GMRF). Two main steps are involved in the edge detection process. The first is the detection step whose main function is to have a high detection rate for all possible non-edge pixels in the image. This detection is based on a generalized pseudo-likelihood ratio test which is used instead of a generalized likelihood ratio test because of its computational simplicity. The output of the detection step is an image which consist of regions separated by fat or thick edges (ambiguity region). To each connected region a label is allocated. The second step involves the localization of the edges. For each connected labeled region obtained from step 1, the GMRF parameters are estimated and stored. To locate an edge between any two regions, we consider the edge regions found in step 1, and find the response with the highest likelihood in the ambiguity region. The method is illustrated on both synthesized textured images and images of outdoor natural scenes.

I. Introduction

Edge detection is an important problem in image segmentation. The traditional methods of edge detection based on the sudden changes in intensity fail in the case of textured images, as they can not differentiate between a "micro-edge" caused by the texture from the "macro-edge" which constitutes a boundary between two textured regions.

Edge-based segmentation of textured images has not been extensively treated. Kashyap and Eom [1] proposed an edge detection algorithm that deals with textured images. First all sharp edges are found, then they are tested as true egdes or just micro edges caused by the texture. Khotanzad and Chen [2] used a simultaneous autoregressive process (SAR) to model the textures, and used a sobel edge operator based on the estimates for the model parameters.

In this paper, we present a new edge detection algorithm which is capable of dealing with both "intensity edges" and "texture edges". We assume here the textured images are modeled by Gaussian Markov Random Fields (GMRF's). The generalization to other stochastic models, such as 2-D causal autoregressive models, simultaneous autoregressive models, etc., is straight forward.

II. Gaussian Markov Random Fields (GMRF)

Let $g_o(m,n)$ be the intensity at pixel $\mathbf{r} = (m, n)$, and let $g(m, n) = g_o(m,n) - \mu$, with $\mu = E\{g_o(m,n)\}$. The GMRF is a noncausal 2D autoregressive process described by the following difference equation

$$g(\mathbf{r}) = \sum_{\mathbf{v} \in D_p} \beta_{\mathbf{r}-\mathbf{v}}\, g(\mathbf{v}) + n(\mathbf{r}) \qquad (2.1)$$

where $\beta_{\mathbf{r}-\mathbf{v}} = \beta_{-(\mathbf{r}-\mathbf{v})}$, and D_p is a neighbor set given by

$$D_p = \{\mathbf{v} = (k, l) : \|\mathbf{r} - \mathbf{v}\|^2 \le N_p \text{ , and } \mathbf{v} \neq \mathbf{r}\} \qquad (2.2)$$

where p is the order of the process and N_p the maximum square of the distance from point $\mathbf{r}$ to $\mathbf{v}$. $\{n(\mathbf{r})\}$ is a Gaussian noise sequence with zero mean and autocorrelation function given by

$$R_n(\mathbf{r}, \mathbf{v}) = \begin{cases} \sigma^2, & \text{if } \mathbf{v} = \mathbf{r} \\ -\sigma^2 \beta_{\mathbf{r}-\mathbf{v}}, & \text{if } \mathbf{v} \in D_p \\ 0, & \text{otherwise} \end{cases} \qquad (2.3)$$

The power spectral density associated with g(m,n) is given by [3]

$$S(\Omega_1, \Omega_2) = \sigma^2 / \left[1 - \sum_{(k,l) \in D_p} \beta_{k,l} \exp\{-j(k\Omega_1 + l\Omega_2)\}\right] \qquad (2.4)$$

The GMRF is parametrized by a parameter set $\gamma = (\mu, \sigma^2, \beta)$, with $\beta = (\beta_{10}, \beta_{01}, \beta_{11}, \beta_{1,-1}, ..)$ where the number of β parameters is determined by the order p of the model.

Let $\mathbf{g}_o = \{g_o(m, n), -N/2 \le m,n \le N/2 - 1\}$ be an NxN image obtained from the infinite extent GMRF $g_o(m,n)$. The joint density function of $\mathbf{g}_o$ is

$$p(\mathbf{g}_o|\gamma) = (2\pi\sigma^2)^{-M/2} \sqrt{\det\{[\psi]\}} \exp\{-(1/2\sigma^2)(\mathbf{g} - \mu\mathbf{1})^\dagger [\psi] (\mathbf{g} - \mu\mathbf{1})\} \qquad (2.5)$$

where $\mathbf{U} = \mu\mathbf{1}$ is the mean vector, $[\Sigma]$ is the covariance matrix of $\mathbf{g}$, $[\Sigma]^{-1} = [\psi]/\sigma^2$, $M = N^2$, and $\dagger$ stands for the transpose operation. Assuming a toroidal lattice results into a random field which is wrapped around in a torus structure [4, 5]. and a covariance matrix $[\Sigma]$ that is circulant. Let $\mathbf{G} = \{G(m, n), -N/2 \le m,n \le N/2 - 1\}$ be the 2D N-point discrete Fourier transform of $\mathbf{g}$, where $\mathbf{g} = \mathbf{g}_o - \mathbf{U}$. G(m, n) is defined as

$$G(m,n) = \sum_{k=-N/2}^{N/2-1} \sum_{l=-N/2}^{N/2-1} g(k, l) \exp\{-j(2\pi/N)[mk + nl]\} \qquad (2.6)$$

$\mathbf{G}$ is a white (used here in the context of having the G(m, n) variables of the random field $\mathbf{G}$ being statistically independent) zero mean Gaussian field (see [4, 5]), with the variance of G(m, n) being $N^2 S(m, n)$, where S(m, n) is obtained from $S(\Omega_1, \Omega_2)$ in (2.4) by evaluating it at $\Omega_1 = 2\pi m/N$, and $\Omega_2 = 2\pi n / N$, and is given by

$$S(m,n) = \sigma^2 / \left[1 - 2 \sum_{(k,l) \in D'_p} \beta_{k,l} \cos\{(2\pi/N)[mk + nl]\}\right] \qquad (2.7)$$

where D'_p is non-symmetric half plane neighborhood set associated the set D_p in (2.2). $p(g|\gamma)$ is given by

$$p(g|\gamma) = \prod_{-N/2 \le m,n \le N/2-1} (1/2\pi N^2 S(m,n))^{1/2} \exp\{-\Sigma |G(m,n)|^2 / 2N^2 S(m,n)\} \qquad (2.8)$$

Finally, under a torus structure [5]

$$\det\{[\psi]\} = \prod_{-N/2 \le m,n \le N/2-1} (\phi(m, n) / N^2) \qquad (2.9)$$

with $\phi(m,n)$ given as

$$\phi(m,n) = \left[1 - 2 \sum_{(k,l) \in D'_p} \beta_{k,l} \cos\{(2\pi/N)[mk + nl]\}\right] \qquad (2.10)$$

II.1 Sufficient Statistics for the GMRF Model

The class of GMRF introduced belongs to the exponential type family, and therefore their likelihood function is factorizable in the Neyman-Fisher sense [6, 7], i.e.,

$$p(g|\gamma) = p(g|\eta) = h(g) \exp\{\mathbf{T}^\dagger \eta + c(\eta)\} \qquad (2.11)$$

where $h(g) = 1$; η is the (2p+2) dimensional natural parameter vector $(\eta_1, \eta_{00}, \eta_{10}, \eta_{01}, \eta_{11}, \eta_{1,-1}, ...) = (\mu N^2/\sigma^2[1 - 2\beta_{10} - 2\beta_{01} - 2\beta_{11} - 2\beta_{1,-1} - ...], -N^2/2\sigma^2, N^2\beta_{10}/\sigma^2, N^2\beta_{01}/\sigma^2, N^2\beta_{11}/\sigma^2, N^2\beta_{1,-1}/\sigma^2, ...)$; $\mathbf{T} = (T_1, T_2, ..., T_{2p+2}) = (\mu^*, R^*_{00}, R^*_{10}, R^*_{01}, R^*_{11}, R^*_{1,-1}, ...)$ is the set of minimal sufficient statistics with μ^* and $R^*_{m,n}$ being the sample mean and sample autocorrelation in the (m, n) direction, respectively; and

$$c(\eta) = 0.5 \log\{\det\{[\Sigma]^{-1}\}\} + \eta_1^2 / 4 [\eta_{00} + \eta_{10} + \eta_{01} + \eta_{11} + \eta_{1,-1} + ...] \qquad (2.12)$$

Under a torus assumption $\det\{[\Sigma]^{-1}\}$ is given as

†This work was partially supported by the National Science Foundation under grant number IRI-8913958 and by the National Institute of Health under grant number 861712.

$$0.5\log\{\det\{[\Sigma]^{-1}\}\} = -N^2\log\{N^2/2\} + 0.5\sum_{-N/2\le m,n\le N/2-1}\log\{-\sum_{(k,l)\in D'_p} \eta_{k,l}\cos\{(2\pi/N)[mk+nl]\}\} + U(0,0) \quad (2.13)$$

Since $c(\eta)$ has partial derivatives of all orders, it follows that [7]

$$E\{T_i\} = -\partial c(\eta)/\partial\eta_i,\ i = 1, 2, .., 2p+2 \quad (2.14)$$

$$\mathrm{cov}\{T_i, T_j\} = -\partial^2 c(\eta)/\partial\eta_i\,\partial\eta_j,\ i, j = 1, 2, .., 2p+2 \quad (2.15)$$

$$E\{T\} = (\mu, R_{00}, R_{10}, R_{01}, R_{11}, R_{1,-1}, ...) \quad (2.16)$$

where

$$R_{kl} = \mu^2 + C_{kl}$$

and

$$C_{k,l} = (1/N^2)\sum_{-N/2\le i,\, j\le N/2-1} S_{i,j}\cos\{(2\pi/N)[ik+jl]\} \quad (2.17)$$

$\mathrm{var}\{\mu^*\}$ and $\mathrm{cov}\{R^*_{k,l}, \mu^*\}$ are given respectively as

$$\mathrm{var}\{\mu^*\} = S_{00}/N^2 \quad (2.18)$$

$$\mathrm{cov}\{R^*_{k,l}, \mu^*\} = 2\mu S_{00}/N^2 \quad (2.19)$$

Finally, $\mathrm{cov}\{T_i, T_j\}$ is given as

$$\mathrm{cov}\{R^*_{k,l}, R^*_{m,n}\} = (2/N^2)[2\mu^2 S_{00} + (1/N^2)\sum_{-N/2\le i,j\le N/2-1}(S_{i,j})^2\cos\{(2\pi/N)[ik+jl]\}\cos\{(2\pi/N)[im+jn]\}] \quad (2.20)$$

Another possible set of sufficient statistics is the set $T' = (\mu^*, C^*_{00}, C^*_{10}, C^*_{01}, C^*_{11}, C^*_{1,-1}, ...)$, where $C^*_{k,l}$ is the sample autocovariance in the (k,l) direction.

$$E\{C^*_{k,l}\} = C_{k,l} - (1/N^2)\sum_{-N/2\le m,n\le N/2-1} C_{m,n} = C_{k,l} - (1/N^2)S_{00} \quad (2.21)$$

where $C_{k,l}$ is given in (2.17). Moreover,

$$\mathrm{cov}\{C^*_{k,l}, \mu^*\} = 0 \quad (2.22)$$

where $C_{m,n}$ is expressed in terms of the $S_{i,j}$'s as in (2.17). Finally,

$$\mathrm{cov}\{C^*_{k,l}, C^*_{m,n}\} = 2(S_{00}/N^2)^2 + (2/N^4)\sum_{-N/2\le i,j\le N/2-1}(S_{i,j})^2\cos\{(2\pi/N)[ik+jl]\}\cos\{(2\pi/N)[im+jn]\} \quad (2.23)$$

From (2.21) we can see that $C^*_{k,l}$ is asymptotically unbiased. In [9] $T' = (\mu^*, C^*_{00}, C^*_{10}, C^*_{01}, C^*_{11}, C^*_{1,-1}, ...)$ is shown to be asymptotically Gaussian with mean vector $E\{T'\} = \mu_{T'} = (\mu, C_{00} - (1/N^2)S_{00}, C_{10} - (1/N^2)S_{00}, C_{01} - (1/N^2)S_{00}, C_{11} - (1/N^2)S_{00}, C_{1,-1} - (1/N^2)S_{00}, ...)$ and covariance matrix $[\Sigma_{T'}]$ having its elements given in (2.18), (2.22), and (2.23).

II.3 Maximum Likelihood Parameter Estimation

The ML estimates for the parameters can be obtained by either maximizing the $\ln\{p(g|\gamma)\}$ using (2.8) as reported in [5], or maximizing (2.11). This involves a nonlinear maximization process such as Newton-Raphson. In terms of the sufficient statistics, the MLE for σ^2 is given by

$$\sigma^{2*} = R^*_{00} - 2\sum_{(k,l)\in D'_p}\beta^*_{kl} R^*_{kl} \quad (2.24)$$

The ML for β the is obtained by maximizing

$$\max_{\beta}\left\{\sum_{0\le m,n\le N-1}\sum \ln\{\phi(m,n)\} - N^2\ln\{1 - 2\sum_{(k,l)\in D'_p}\beta_{kl}\rho^*_{kl}\}\right\} \quad (2.25)$$

where $\phi(m,n)$ is given in (2.10) and ρ^*_{kl} is defined as

$$\rho^*_{kl} = R^*_{kl}/R^*_{00} \quad (2.26)$$

The MLE is unique [7]. The parameters should satisfy the following stability condition to correspond to a GMRF

$$2\sum_{(k,l)\in D'_p}\beta_{k,l}\cos\{(2\pi/N)[mk+nl]\} < 1,\ \text{for } -N/2 \le m, n \le N/2-1 \quad (2.27)$$

III. Pseudo-Likelihood Function

The pseudo-likelihood function is the product of the conditional likelihoods of the image intensity data over the entire image lattice Ω of size NxN, i.e.,

$$Pl(g|\gamma) = \prod_{r\in\Omega} p(g(r)|\, g_{(r)}, \gamma) = \prod_{r\in\Omega} p(g(r)|\, g(r), v\in D_p, \gamma) \quad (3.1)$$

where $g_{(r)}$ is the data vector not including the data at pixel r. In [8] it is shown that the Kullback-Leibler information (KLI) [7] based on pseudo-likelihood function is unbiased, i.e.,

$$E\left\{\log\{Pl(g|\gamma)/Pl(g|\gamma_{true})\}\right\} \le 0 \quad (3.2)$$

where γ_{true} is the true parameter set. Moreover, it is shown [8] that the $p(KLI > 0) \to 0$ as $N\to\infty$, i.e.,

$$p\left(\lim_{N\to\infty}\ln\{Pl(g|\gamma)/Pl(g|\gamma_{true})\} > 1\right) = 0 \quad (3.3)$$

Pseudo-likelihood parameters estimates are obtained by maximizing (3.1). They were shown [5] to be consistent estimators and asymptotically efficient. The pseudo-likelihood estimator for β is a least square type estimator and takes the form [5]

$$\beta_{Pl} = \left[\sum_{r\in\Omega} X^{\dagger}(r)X(r)\right]^{-1}\sum_{r\in\Omega} X(r)\, g(r), \quad r = (i, j) \quad (3.4)$$

where $X(r) = (g(i-1, j) + g(i+1, j), g(i, j-1) + g(i, j+1), ...)$. The pseudo-likelihood for σ^2 is given by

$$\sigma^2_{Pl} = (1/N^2)\sum_{r\in\Omega}[g(r) - \beta_{Pl}X(r)]^2 \quad (3.5)$$

The pseudo-likelihood estimate for the parameter vector γ is denoted as $\gamma_{Pl} = (\sigma^2_{Pl}, \beta_{Pl})$. The drawback associated with the pseudo-likelihood estimators is that they are not guaranteed to satisfy the stability condition in (2.27). This condition is necessary for the MRF to be Gaussian.

IV. Detection of Non-Edge Pixels

Two main steps are involved in our edge detection scheme. The first is the detection-step whose main function is to have a high detection rate for all possible non-edge pixels in the image.

To detect a non-edge at pixel (i, j), we have considered the following two groups of analysis edge detector windows centered at pixel (i, j) shown in Figure 1.

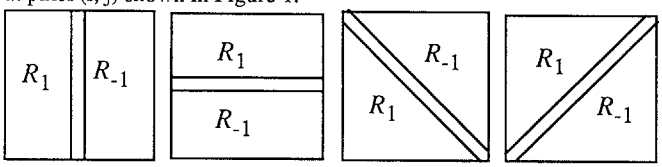

Horizontal Vertical Diagonal 1 Diagonal 2

Analysis windows

Figure 1

Let $R_1(k)$ and $R_{-1}(k)$ denote the set of pixels labelled 1 and -1, respectively, for window k (k = horizontal, vertical, diagonal 1, diagonal 2). Let M_1 and M_{-1} ($M_1 = M_{-1}$) be the number of pixels in regions $R_1(k)$ and $R_{-1}(k)$, respectively, and $M = M_1 + M_{-1} = 2M_1$. Let H_0 be the hypothesis that there is no edge (at pixel (i, j), and H_a be the hypothesis that there is edge at pixel (i, j).

Remark:

Analysis windows with different directions could also be used.

IV.1 Likelihood Ratio Test

Let $g_1(k)$ and $g_{-1}(k)$ be the data in regions $R_1(k)$ and $R_{-1}(k)$, respectively. H_0 translates into $g_1(k)$ and $g_{-1}(k)$ having the same distributions, i.e., $\gamma_1 = \gamma_{-1} = \gamma_o$, and H_1 translates to $\gamma_1 \ne \gamma_{-1}$. The generalized likelihood ratio test [7] statistic is

$$L(g_1(k), g_{-1}(k)) = \ln\left\{p(g_1(k)|\gamma_1^*)p(g_{-1}(k)|\gamma_{-1}^*)/p(g_1(k), g_{-1}(k)\,|\,\gamma_o^*)\right\} \quad (4.1)$$

where γ_1^* and γ_{-1}^* are the MLE of γ based on the data $g_1(k)$ and $g_{-1}(k)$, respectively; and γ_o^* is the MLE of based on the data $g_o(k) = g_1(k) \cup g_{-1}(k)$. It can be easily shown that

$$p(g_c(k)\,|\,\gamma_c^*) = (2\pi\sigma_c^{*2})^{-M_c/2}(\det[\psi^*_c])^{1/2}\exp\{-M_c/2\},\quad c = 1, -1 \quad (4.2)$$

$$p(g_o(k)\,|\,\gamma_o^*) = (2\pi\sigma_o^{*2})^{-M/2}(\det[\psi^*_o])^{1/2}\exp\{-M/2\} \quad (4.3)$$

Hence (4.1) becomes

$$L(g_1(k), g_1(k)) = 1/2\ln\{\det\{[\psi^*_1]\}\det\{[\psi^*_1]\}/\det\{[\psi^*_o]\}\} + M_1/2\log\{\sigma_o^{*4}/\sigma_1^{*2}\sigma_{-1}^{*2}\} \quad (4.4)$$

For large M, under H_0, $L(g_1(k), g_{-1}(k))$ in (4.1) has a χ^2 distribution with 2p+2 degrees of freedom [7].

H_0 is rejected if

$$\log\{\det\{[\psi^*_1]\}\det\{[\psi^*_{-1}]\}/\det\{[\psi^*_o]\}\} + M_1\ln\{\sigma_o^{*4}/\sigma_i^{*2}\sigma_j^{*2}\} > \xi_\alpha \quad (4.5)$$

with ξ_α chosen such that the size of the test is α. Under a torus

lattice approximation, $\det\{[\psi^*_c]\}$, c = i, j, is given in (2.9), where $\phi^*_c(m, n)$ is given in (2.10) with $\beta^{c*}_{k,l}$ replacing $\beta_{k,l}$ in (2.10), and $M_c = N^2$; whereas $\det\{[\psi^*_o]$ is given in (2.9), with $\phi^*_o(m, n)$ given in (2.10) with $\beta^{o*}_{k,l}$ replacing $\beta_{k,l}$ in (2.10), and $M = N^2$. $\beta^{o*}_{k,l}$ is the MLE for $\beta^o_{k,l}$ obtained from the data $\mathbf{g}_o(k) = \mathbf{g}_1(k) \cup \mathbf{g}_{-1}(k)$.

The only drawback associated with the generalized likelihood ratio test is the fact that the MLE for γ_1, γ_{-1} , and γ_o are to be evaluated, and this requires a time-consuming nonlinear hill-climbing technique. Computationally simpler alternatives are presented next.

Remark :

The pseudo-likelihood estimators can not be used in the likelihood ratio test as they are not guaranteed to satisfy the stability condition in (2.27).

IV.2 Generalized Pseudo-Likelihood Ratio Test

As an alternative to the the likelihood ratio test, we use the following pseudo-likelihood ratio test

$$Pl(\mathbf{g}_1(k), \mathbf{g}_{-1}(k)) = Pl(\mathbf{g}_1(k)|\gamma_{Pl,1})\, Pl(\mathbf{g}_{-1}(k)|\gamma_{Pl,-1}) \,/\, Pl(\mathbf{g}_1(k), \mathbf{g}_{-1}(k)|\gamma_{Pl,o}) \quad (4.6)$$

Taking the log of (4.9) yields

$$PL(\mathbf{g}_1(k), \mathbf{g}_{-1}(k)) = N_1/2 \ln\{\sigma_{Pl,o}{}^4 / \sigma_{Pl,1}{}^2\, \sigma_{Pl,-1}{}^2\} \quad (4.7)$$

The success of such a test is due to the fact that the pseudo-likelihood function is unbiased, and that the $p(KLI > 0) \rightarrow 0$ as $N \rightarrow \infty$ (see Section II.3). For large N, under H_o, $\sigma_{Pl,o}{}^2 / \sigma_{Pl,1}\, \sigma_{Pl,-1}$ has an F distribution, i.e., $(\sigma_{Pl,o}{}^2 / \sigma_{Pl,1}\, \sigma_{Pl,-1}) \sim F(2p+2, 2p+2)$.

H_o is rejected if

$$\{\sigma_{Pl,o}{}^2 / \sigma_{Pl,1}\, \sigma_{Pl,-1}\} > \xi_\alpha \quad (4.8)$$

with ξ_α chosen such that the size of the test is α.

V. Edge Localization

The output of the detection step above is an image which consist of regions separated by fat or thick edges (ambiguity region). To each connected region a label is allocated. For each labelled region we estimate the parameters of the GMRF associated with that region. The MLE are now obtained via (2.27) and (2.28), but with the R^*_{kl}'s computed based on summing product terms of the form g(m, n)g(m+ k, n + l) with both points belonging to the region.

V.1 Maximum Likelihood Edge Location Estimation

To locate an edge between any two regions, we consider the edge regions found in step 1, and find the strongest response (the response with the highest likelihood) associated with the edge location in the ambiguity region. For example, suppose we consider the situation shown in Figure 2. The two non-edge regions are denoted by R_I and R_{II}, respectively. Let γ^*_m (η^*_m), m = I, II, be the estimated GMRF parameters associated with regions R_I and R_{II}, respectively.

To detect the vertical edge in the ambiguity region associated with the ith row, we compute the likelihood functions associated with all the possible locations of the vertical edge in the ith row which are in the ambiguity region. If the ambiguity region associated with the ith row has a width of W pixels, with j set to 0 and W at the begining and end of the ambiguity region, there will be (W+1) such computations. For each possible (i, j) location of the edge, we use an analysis window of size L such as the one shown in Figure 2 centered at the (i, j) point.

We compute the sufficient statistics vector $\mathbf{T'}_1(i, j)$ and $\mathbf{T'}_{-1}(i, j)$ based on the data in regions $R_1(k)$ and $R_{-1}(k)$, respectively. Using (2.11) the log likelihood of the data in regions $R_1(k)$ and $R_{-1}(k)$ centered at point (i, j) reduces to

$$\mathbf{T'}_1(i, j)^\dagger \eta^*_I + c(\eta^*_I) + \mathbf{T'}_{-1}(i, j)^\dagger \eta^*_{II} + c(\eta^*_{II}) \quad (5.1)$$

We slide the window from one end of the ambiguity region to the other end, i.e., j = 0 to W. The location of the edge in the ambiguity region is the one for which (5.1) is a maximum. The decision rule is

$$\max_j \{\mathbf{T'}_1(i, j)^\dagger \eta^*_I + \mathbf{T'}_{-1}(i, j)^\dagger \eta^*_{II}\} \quad (5.2)$$

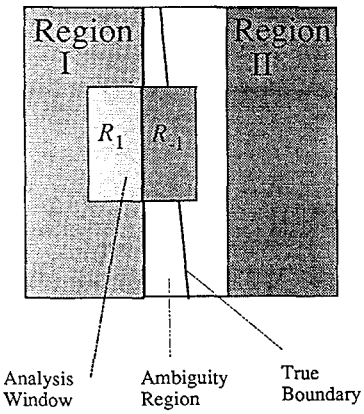

Figure 2

Remark : The ML is biased for small size analysis windows (see experiment Section).

V.2 Localization of the Edge by Maximizing the SNR

An alternative to the ML edge location in Section V.1 is based on maximizing the likelihood function associated with the difference $\Delta\mathbf{T}(i, j) = (\mathbf{T'}_1(i, j) - \mathbf{T'}_{-1}(i, j))$. Let $\mu^*_{T'}(m)$ and $[\Sigma^*_{T'}(m)]$, m = I, II, be the estimated mean and covariance matrix associated with the sufficient statistics $\mathbf{T'}$ associated with regions R_I and R_{II}, respectively. These are computed using (2.21), (2.22), and (2.23). Using the Gaussian approximation for the probability density function of the sufficient statistics, the edge location is achieved by the following ML maximization rule

$$\max_{0 \le j \le W} \{p(\Delta\mathbf{T'}(i, j)|\Delta\mu_{T'}, [\Delta\Sigma_{T'}])\} \quad (5.3)$$

where

$$\Delta\mu_{T'} = \mu^*_{T'}(I) - \mu^*_{T'}(II) \quad (5.4)$$

and

$$[\Delta\Sigma_{T'}] = [\Sigma^*_{T'}(I)] + [\Sigma^*_{T'}(II)] \quad (5.5)$$

(5.3) reduces to

$$\max_{0 \le j \le W} \{(\Delta\mathbf{T'}(i, j) - \Delta\mu_{T'})^\dagger [\Delta\Sigma_{T'}]^{-1} (\Delta\mathbf{T'}(i, j) - \Delta\mu_{T'})\} \quad (5.6)$$

The decision rule in (5.3) was found to perform better than its counterpart in (5.2) for analysis windows which are of small sizes (see experiment section).

Remark :

The decision rule is maximizing the between-to-within variation, which is a measure of the signal-to-noise ratio.

IV. Experiments

Experiments have been conducted on both natural and synthetic scenes images. Figure 3a shows a synthesized image which consists of 4 regions which are realizations of 4 different second order GMRF's. The output of the detection step is shown in Figure 3b. In Figure 3c each connected non-edge region has been allocated a label (a constant shade of gray) and the edge-ambiguity region is displayed in white. For each labelled region the GMRF parameters were estimated. Based on these estimated parameters, the output of the localization step is shown in Figure 3d. The localization step is based on the decision rule outlined in Section V.2.

The same steps are shown for two real images. The first taken in our Laboratory is an image of three different fabrics. The original image and the different results of the segmentation process are shown in Figures 4a-4d. Fourth order GMRF's were used here. The second image is that of outdoor scene which consists of two regions : earth region, and grass region. The results are shown in Figures 5a-5d.

In all the three images, the results were good, and most edges between regions were properly localized to within a pixel of the true boundary. Moreover, most the "micro-edges" caused by the texture have been neglected.

We finally compare the performance of the decision rules in Section V.1 and V.2 as a function of analysis window size for the example shown in Figure 6. Only a horizontal analysis window was used here. The output of the decision in (5.2) for three analysis windows of sizes 20x16, 40x30, and 60x40, respectively, are shown in Figures 7a, 7b, and 7c. This is to be contrasted with the outputs using the decision rule in (5.6), which are shown in Figures 8a, 8b, and 8c.

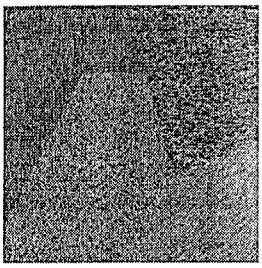

Figure 3a

Figure 3b

Figure 3c

Figure 3d

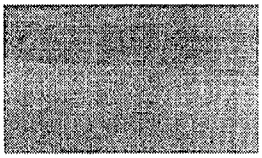

Figure 4a

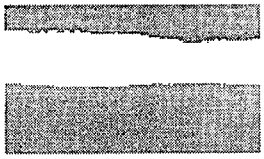

Figure 4b

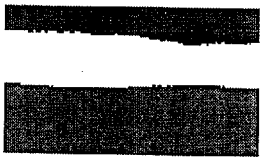

Figure 4c

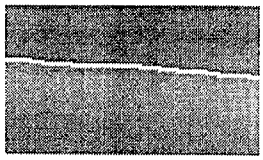

Figure 4d

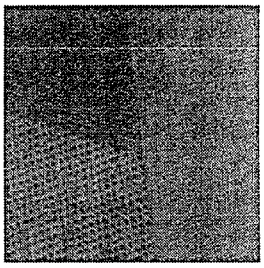

Figure 5a

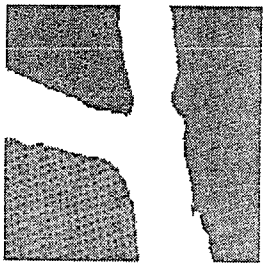

Figure 5b

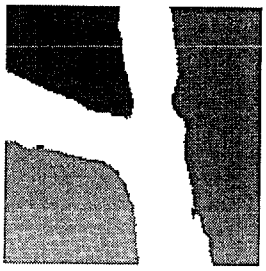

Figure 5c

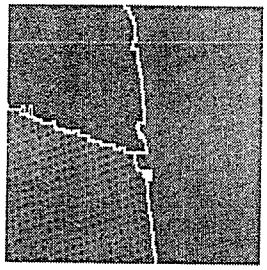

Figure 5d

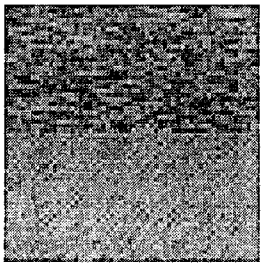

Figure 6a

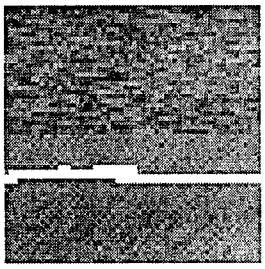

(a)

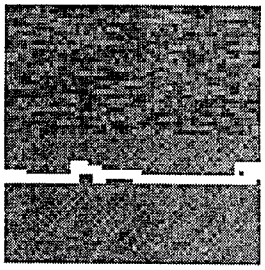

(b)
Figure 7

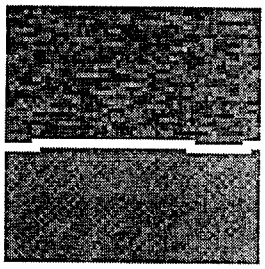

(c)

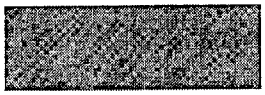

Figure 6b

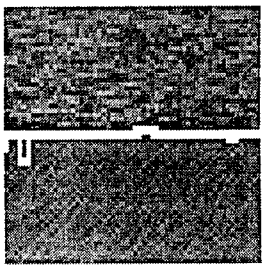

(a)

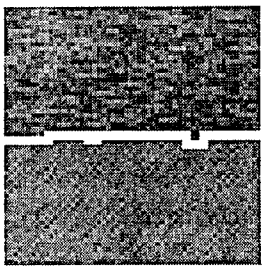

(b)
Figure 8

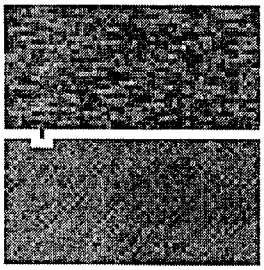

(c)

References

[1] [R. Kashyap and K. Eom, "Texture Boundary Detection using Long Correlation Model," Proc. of the 21st Allerton Conf., Chicago, Oct. 1983.

[2] A. Khotanzad and J. Y. Chen, "Unsupervised Segmentation of Textured Images by Edge Detection in Multidimensional Feature," IEEE Trans. on Pattern Analysis and Machine Intelligence, vol. PAMI-11, April 1989.

[3] J. Woods, "Two-Dimensional Discrete Markov Random Fields," IEEE Trans. Information Theory, vol. IT-18, 1972.

[4] J. Besag and P. Moran, "On the Estimation and Testing of Spatial Interaction in Gaussian Lattices," Biometrika, Vol. 62, 1975.

[5] R. Kashyap and R. Chellappa, "Estimation and Choice of Neighbors in Spatial Interaction Models of Images," IEEE Trans. Information Theory, Jan. 1983.

[6] R. Chellappa and S. Chatterjee, "Texture Classification using GMRF Models," IEEE Trans. on ASSP, August 1985.

[7] S. Zacks, *Parametric Statistical Inference*, Pergamon Press, London, 1981.

[8] F. Cohen and D. Cooper, "Simple Parallel Hierarchical and Relaxation Algorithms for Segmenting Noncausal Markov Random Fields," IEEE Trans. on Pattern Analysis and Machine Intelligence, Vol. PAMI-9, No. 2, March 1987.

[9] Z. Fan and F. Cohen, "Textured Image Segmentation as a Multiple-Hypothesis Test," IEEE Trans. on Systems and Circuits, Vol. 35 No. 6, June 1988.